American Mineralogist, Volume 75, pages 813–824, 1990

Serpentinization of enstatite from Pernes, France: Reaction microstructures and the role of system openness

Maïté Le Gleuher*
Université d'Aix-Marseille III, Marseille, France
Kenneth J. T. Livi, David R. Veblen
Department of Earth and Planetary Sciences, The Johns Hopkins University, Baltimore, Maryland 21218, U.S.A.
Yves Noack
Géosciences des Environnements Tropicaux, Faculté de St-Jérôme, Université d'Aix-Marseille III, Marseille, France
Marc Amouric
Centre de Recherche sur les Mécanismes, de la Croissance Cristalline, CNRS, Campus Luminy, Marseille, France

Abstract

Partially serpentinized enstatite porphyroblasts and entirely serpentinized matrix grains from the pyroxenite at Pernes, France, were studied with high-resolution and analytical transmission electron microscopy. The enstatite alteration resulted in two different textures: (1) topotactic aluminous lizardite, with five lizardite layers replacing two enstatite cells, $(001)_{liz} \parallel (100)_{en}$; and (2) randomly oriented packets of lizardite mixed with polygonal serpentine, chrysotile, curved serpentines, chlorite, and mixed-layer silicates. The first texture is due to a reaction involving Al-Si tetrahedral substitutions, Mg-Al and Fe^{2+}-Al octahedral substitutions, a net gain of approximately 40% Al per unit volume, and moderate structural modifications. The lizardite apparently inherits part of the pyroxene structure. In the second texture, pyroxene does not control the orientation of the alteration products. The pyroxenes are dissolved, and the serpentines and other sheet silicates crystallize from the fluid. Topotactic lizardite occurs in relatively closed microenvironments (areas of restricted fluid flow), whereas the randomly oriented products tend to occur in more open environments such as the matrix, areas cut by fractures, and regions of concentrated defects at the interfaces of augite exsolution lamellae. These textures suggest that the degree of openness of the system may be significant in determining the mechanisms of the alteration reactions.

Introduction

Studies of the alteration and weathering of pyroxenes have resulted in two main types of hypothesized reaction mechanisms: (1) topotactic reactions in the sense of Oswald and Günter (1985), commonly called solid-state reactions, even though a fluid obviously is also involved (Velbel, 1987; Veblen and Buseck, 1980, 1981; Nakajima and Ribbe, 1980; Eggleton and Boland, 1982); and (2) dissolution-neoformation reactions (Colin et al., 1985; Delvigne, 1983; Nahon and Colin, 1982). The divergent conclusions result, in part, from different scales of observation and from the investigation of different alteration environments. Several workers have described the mineralogy and textures of pseudomorphic serpentine after pyroxene (bastites) using optical microscopy and X-ray diffraction (Wicks and Whittaker, 1977; Wicks and Plant, 1979). They found that the serpentine consists of lizardite *1T* with minor amounts of two-layer lizardite and chrysotile. (The name chrysotile is used in this paper to refer to serpentine minerals with rolled or circular morphology.) Transmission electron microscopy (TEM) studies of bastites have revealed the additional occurrence of polygonal serpentine, curved serpentine structures, chlorite, and talc (Cressey and Zussman, 1976; Cressey, 1979; Veblen and Buseck, 1979, 1981; Spinnler, 1985; Wicks, 1986).

The first TEM studies of the crystallographic relationships between bastite and its parent minerals were conducted by Cressey (1977, 1979) on samples characterized by Wicks and Whittaker (1977). Cressey (1979) observed that enstatite and augite exsolution lamellae alter mainly to fine-grained serpentine without any preferred orientation. However, in a few well-crystallized regions, (001) of lizardite was nearly parallel to the (100) enstatite. According to Cressey, the topotactic lizardite results from recrystallization of the initial poorly crystallized serpen-

* Present address: Centre for Australian Regolith Studies, Department of Geology, Australian National University, GPO Box 4, Canberra, ACT 2601, Australia.

0003–004X/90/0708–0813$02.00

TABLE 1. Average EMP analyses (wt%) and structural formulae of parent minerals and serpentines from the pyroxenite of Pernes

	1	2	3	4	5	6
SiO_2	54.37	50.55	0.00	37.28	35.02	31.52
MgO	31.70	14.34	20.27	32.65	31.51	22.88
FeO	8.19	2.37	11.22	6.74	7.52	7.56
Al_2O_3	5.32	7.71	64.39	8.02	9.37	4.31
CaO	0.25	22.60	0.00	0.18	0.19	9.16
Na_2O	0.04	1.27	0.01	0.04	0.01	0.10
K_2O	0.02	0.00	0.00	0.11	0.09	—
MnO	0.16	0.13	0.02	0.09	0.15	0.02
Cr_2O_3	0.18	0.13	3.55	0.18	0.32	0.24
TiO_2	0.09	0.91	0.03	0.07	0.08	12.97
NiO	—	—	0.09	0.02	0.03	—
Si	0.943	0.918	0.000	1.815	1.741	
Mg	0.819	0.388	0.776	2.370	2.335	
Fe^{2+}	0.119	0.036	0.238	0.274	0.313	
Al	0.109	0.165	1.924	0.460	0.549	
Ca	0.005	0.440	0.000	0.010	0.010	
Na	0.001	0.045	0.000	0.003	0.001	
K	0.001	0.000	0.000	0.007	0.006	
Mn	0.002	0.002	0.000	0.004	0.007	
Cr	0.002	0.002	0.071	0.007	0.013	
Ti	0.001	0.012	0.001	0.003	0.003	
Ni	—	—	0.002	0.001	0.001	
O*	3	3	4	7	7	

Note: 1: average of 6 analyses of enstatite; 2: average of 7 analyses of augite; 3: average of 4 analyses of ferroan spinel; 4: average of 29 analyses of lizardite; 5: average of 7 analyses of serpentine after enstatite grains in the microcrystalline matrix; 6: composition of the Ti- and Ca-rich serpentine in the microcrystalline matrix; O*: assumed number of oxygens; —: not determined; and total iron as FeO.

TABLE 2. EMP analyses (wt%) of pseudomorphic serpentine after pyroxene and of nonpseudomorphic aluminous serpentine

	2	3	4	5	6	7	8
SiO_2	37.80	40.40	38.40	39.77	38.80	39.80	31.10
MgO	36.80	36.90	37.60	37.25	37.20	40.90	29.30
FeO	7.40	3.60	3.60	6.57	3.74		1.90
Al_2O_3	4.10	4.70	5.70	2.23	5.86	4.50	22.20
CaO	0.08		0.12	0.07			0.30
K_2O							1.00
MnO	0.15	0.08	0.04	0.21	0.03		
Cr_2O_3	0.61	0.56	1.05	0.66	0.27		
TiO_2	0.03						
NiO		0.06	0.05	<0.01	0.05		

Note: Total iron as FeO. The numbers of the analyses refer to Figure 2.

tine. Therefore, the pyroxene precursor does not control the initial serpentine orientation. Alternatively, Buseck et al. (1980) suggest that the topotactic lizardite represents the early stage of serpentinization, and the randomly oriented serpentine appears later. Using high-resolution TEM (HRTEM) on specimens previously examined by Wicks and Whittaker (1977) and Wicks and Plant (1979), Spinnler (1985) concluded that the pyroxene-to-serpentine reaction is not rigorously topotactic. Wicks (1986) correlates the results of single-crystal X-ray diffraction and HRTEM on the same samples and calculates that 40% of the lizardite is in a topotactic relationship with enstatite ($\mathbf{a}_{liz} \parallel \mathbf{c}_{en}$, $\mathbf{c}_{liz} \parallel \mathbf{a}_{en}$, $\mathbf{b}_{liz} \parallel \mathbf{b}_{en}$), 45% is randomly oriented, and the rest is in other topotactic orientations, including $\mathbf{a}_{liz} \parallel \mathbf{c}_{en}$, $\mathbf{b}_{liz} \parallel \mathbf{a}_{en}$, $\mathbf{c}_{liz} \parallel \mathbf{b}_{en}$. In addition, Wicks discriminates among the formation of different serpentine minerals on the basis of temperature, prograde-versus-retrograde reactions, and availability of water.

In the present study, we have investigated the possibility of a relationship between the orientation of pyroxene and its alteration products and the microenvironment in which the alteration occurred. Using TEM and analytical electron microscopy (AEM) data, we conclude that in the rocks at Pernes, environments of relatively restricted fluid flow resulted in topotactic lizardite with unusually high Al contents, whereas less restricted environments created predominantly randomly oriented lizardite and other sheet silicates.

EXPERIMENTAL METHODS, SPECIMEN DESCRIPTION, AND ELECTRON MICROPROBE ANALYSES

Methods

HRTEM and AEM investigations were performed with a Philips 420 microscope operating at 120 keV and equipped with an EDAX energy-dispersive X-ray detector and a Princeton Gamma-Tech System IV analyzer. Sample preparation of ion-milled specimens, HRTEM, and AEM analyses followed the procedures described by Livi and Veblen (1987). Electron microprobe (EMP) analyses were obtained with a Cameca Camebax instrument using wavelength dispersive analysis. Scanning electron microscope (SEM) observations were made with a Cambridge Stereoscan 200 equipped with an energy-dispersive detector. X-ray diffractometry (XRD) was performed on both Philips PW 1729 and PW 1730 diffractometers using Co$K\alpha$ radiation with an Fe filter.

Occurrence and petrography

Samples of partially altered pyroxenite were selected from the Massif des Pernes in the Pyrénées Atlantiques, France. The pyroxenite body is intensely cut by two systems of roughly orthogonal fractures that divide the rock into parallelopipeds. Sections of these blocks display a dark green, serpentinized periphery, a mottled zone with dark green altered regions and fresh gray areas, and an unaltered gray core.

The original ultramafic rock consists of 90% enstatite and augite porphyroblasts and 10% fine-grained matrix. The porphyroblasts, up to 6 mm long, can exhibit strain features such as undulatory extinction, stretching, and kink bands, and some of the augite grains are mechanically twinned. The enstatite porphyroblasts contain thin {100} augite exsolution lamellae. The matrix consists of fine-grained pyroxene neoblasts and olive green spinel (ferroan spinel) with relatively low Cr contents. Table 1 presents analyses of the porphyroblasts (analyses 1 and 2) and interstitial spinel (analysis 3).

In the mottled zone, the enstatite and matrix minerals are partially to completely pseudomorphed, primarily to

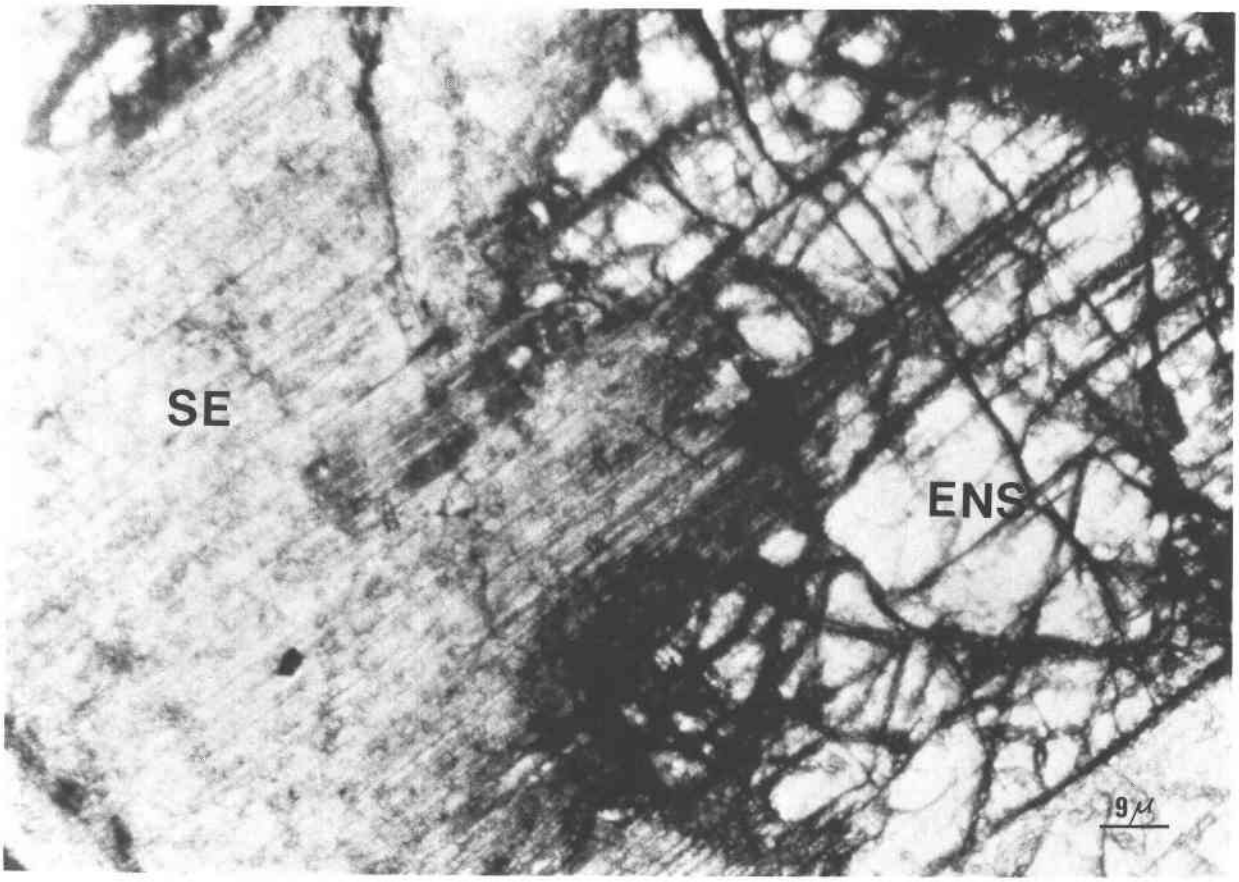

Fig. 1. Optical micrograph (cross-polarized light) of partially serpentinized enstatite. ENS = enstatite; SE = serpentine.

serpentine (Fig. 1), whereas augite remains relatively fresh, except for a few grains that are altered along fractures or twin planes.

The serpentine is pale green in thin section and orange in cross-polarized light. Its growth preserves the original deformation features and cleavage traces of the enstatite porphyroblasts. When observed in the SEM, these altered enstatites exhibit platy morphology characteristic of lizardite. Average microprobe analyses of the pseudomorph lizardite indicates an unusually high alumina content of 8 wt% (Table 1, analysis 4). An average analysis of Pernes pseudomorphic serpentines is presented in Table 1 and plotted in Figure 2 with analyses of pseudomorphic and nonpseudomorphic serpentines from other studies (Table 2).

No other alteration product has been identified by X-ray diffraction or secondary electron imaging, although a few Fe-Ni sulfide minerals have been identified with the SEM. In the mottled zone, partially serpentinized, unstrained enstatite porphyroblasts and entirely serpentinized regions of the surrounding matrix were selected for further study by TEM.

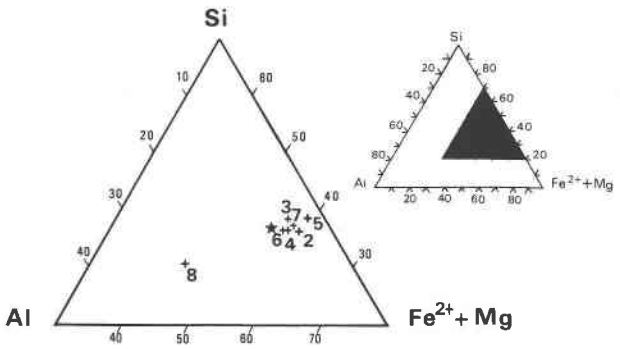

Fig. 2. Compositions of the lizardite of Pernes, of pseudomorphic serpentines after pyroxenes, and of nonpseudomorphic aluminous serpentines, plotted in a Si-Al-(Fe^{2+} + Mg) cation-normalized ternary diagram. The diagram is an expanded view of the shaded area in the small triangle. ⋆ = lizardite, this study; 2 = pseudomorphic lizardite, Wicks and Plant (1979); 3 = pseudomorphic lizardite after orthopyroxene, Dungan (1979); 4 = pseudomorphic lizardite after clinopyroxene, Dungan (1979); 5 = pseudomorphic lizardite, Ikin and Harmon (1983); 6 = nonpseudomorphic lizardite, Frost (1975); 7 = nonpseudomorphic lizardite, Mellini (1982); 8 = nonpseudomorphic serpentine, Jahanbagloo and Zoltai (1968).

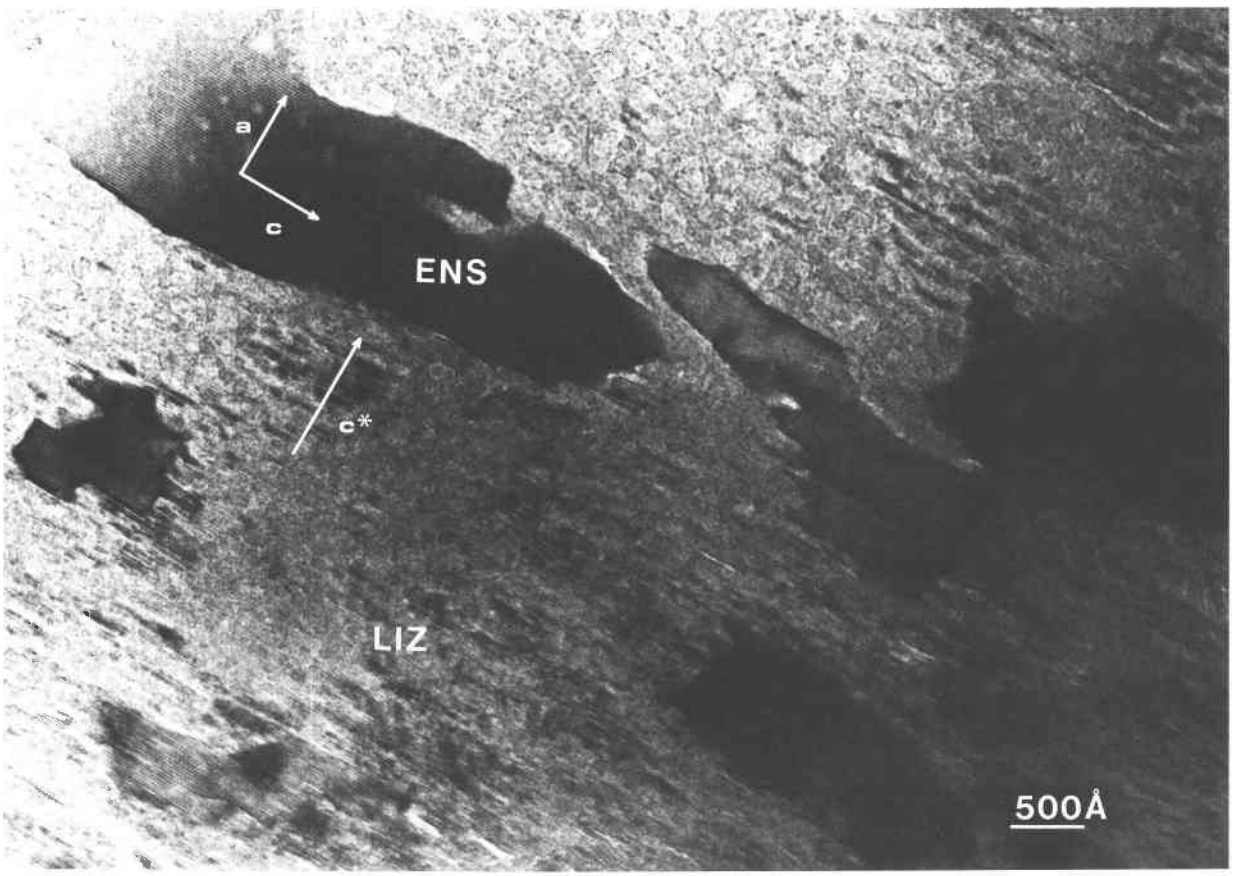

Fig. 3. Bright-field TEM image showing fresh enstatite islands (ENS) scattered in secondary lizardite (LIZ). The long dimensions of the enstatite relicts are parallel to the pyroxene *c* axis.

Lizardite and enstatite unit-cell calculations

Unit-cell parameters, which were used subsequently for calculations of reaction mass balances, were determined from powder X-ray diffraction data with the least-squares program Unit-cell (Tournarie, 1969). The enstatite-bronzite unit-cell parameters were calculated using the indexing from an enstatite reference cell given by Deer et al. (1978) (Table 3). As a literature search failed to produce a well-characterized aluminous lizardite close to the Pernes lizardite composition, the parameters of a reference unit cell were calculated using the regression equations of Chernosky (1975) that relate the variation of cell parameters to the number of moles of Al (x) in the general serpentine formula $(Si_{4-x}Al_x)(Mg_{6-x}Al_x)O_{10}(OH)_8$. The unit cell for the Pernes lizardite was refined on the basis of a one-layer orthorhombic cell with x = 0.6 (which gave the best refinement), and the unit-cell parameters are given in Table 3.

TABLE 3. Enstatite and lizardite unit-cell parameters and reference unit-cell parameters

	Enstatite		Lizardite	
	Reference	Pernes	Reference	Pernes
a Å	18.223	18.261 ± 0.071	5.315	5.318 ± 0.004
b Å	8.815	8.879 ± 0.035	9.212	9.222 ± 0.005
c Å	5.169	5.205 ± 0.018	7.195	7.204 ± 0.014

TEM OBSERVATIONS OF ENSTATITE ALTERATION

Alteration of enstatite porphyroblasts

The enstatite crystal examined by HRTEM exhibits numerous augite exsolution lamellae 500 to 1300 Å wide. Their compositions are similar to those of the augite porphyroblasts. AEM analyses of the enstatite host and the augite lamellae are presented in Table 4 (analyses 1–10). The transition between the enstatite and serpentine is gradual. Near the edge of the altering grain, islands of enstatite occur scattered through the lizardite (Fig. 3). These remnants tend to have their long dimensions parallel to the **c** axis, suggesting that alteration progresses more rapidly parallel to the tetrahedral chains.

A survey of HRTEM images supports X-ray diffraction results showing that one-layer lizardite is the dominant serpentine mineral. Serpentine is rapidly damaged by the electron beam, and thus proper sample orientation for two-dimensional high-resolution lattice imaging is not

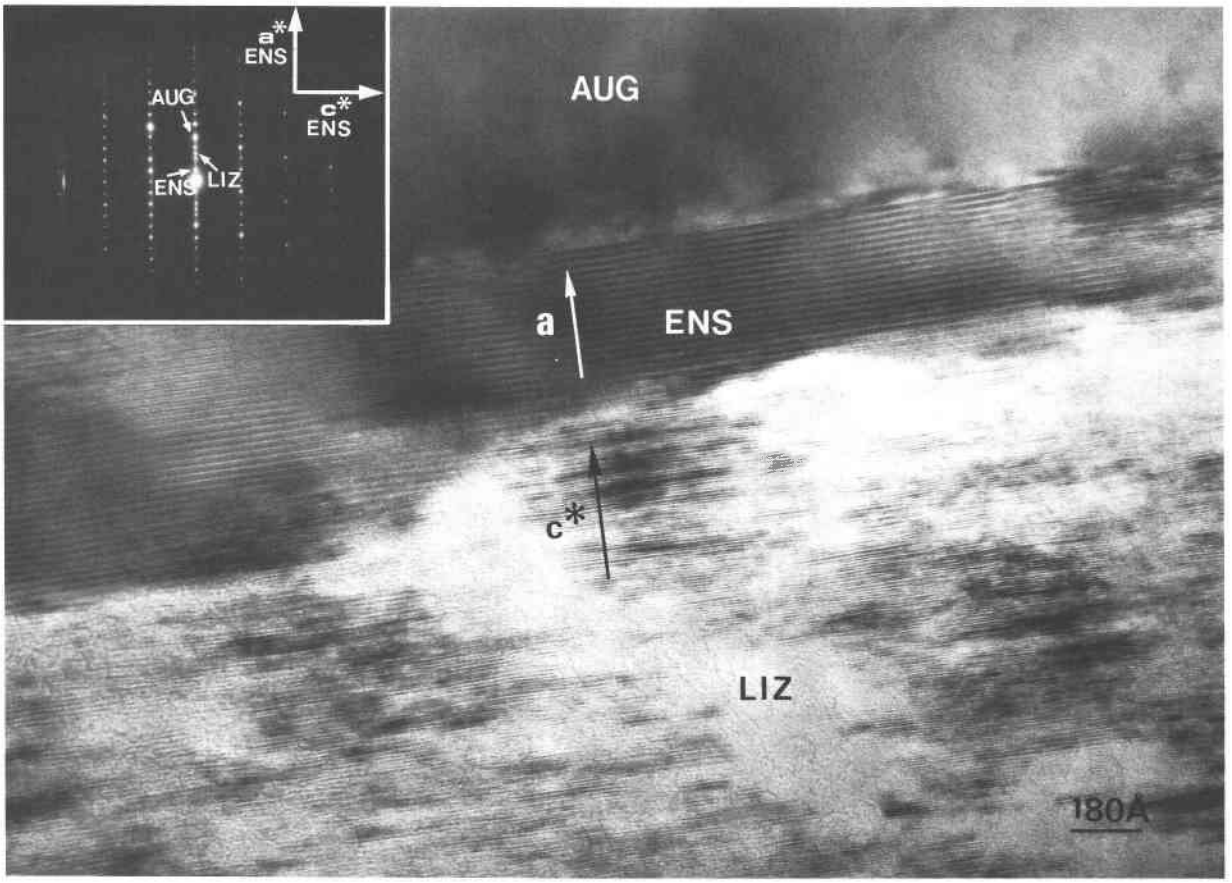

Fig. 4. Lattice-fringe image of a contact between enstatite and topotactic-lizardite. The enstatite (ENS) contains an augite exsolution lamella (AUG). The (001) planes of lizardite are parallel to (100) of enstatite. The inset SAED pattern displays weak streaking along **c*** of lizardite, indicating minor stacking disorder.

possible. However, one-dimensional lattice images are sufficient for distinguishing the types of phases found. The 7.3-Å (001) topotactic-lizardite layers imaged in Figure 4 are roughly parallel to the (100) plane of the nearby enstatite. At the enstatite-lizardite boundary, five lizardite sheets generally replace two 18-Å enstatite cells. Minor stacking disorder is indicated by weak streaking along c^* (see selected area diffraction (SAED) pattern in inset of Fig. 4). This pattern also displays diffraction spots arising from an augite lamella. The orientation relationship commonly breaks down away from the pyroxene boundary. AEM analyses of topotactic lizardite confirm the high Al_2O_3 contents obtained by EMP analysis (Table 4, analyses 11–19).

In addition to planar serpentine, HRTEM observations reveal incomplete chrysotile rolls, serpentine ribbon structures, and curved structures similar to those described by Veblen and Buseck (1979, 1981), Veblen (1980), Spinnler (1985), and Wicks (1986). Figure 5 shows a circumflex structure that consists of serpentine fringes exhibiting large changes in orientation. Unfortunately, AEM analyses are not available to determine if chrysotile rolls and curved structures have similar or lower alumina contents than the topotactic lizardite.

Chrysotile rolls and other curved serpentine structures commonly are associated with chlorite layers and isolated layers of lizardite, talc, and brucite. In the upper part of Figure 5, chlorite has replaced enstatite that previously was host to an augite lamella; the relatively alteration-resistant lamella remains. The chlorite contains polytypic stacking disorder and defects consisting of extra talc-like layers (or missing brucite-like layers). If the orientation of the augite lamella reflects the orientation of the converted enstatite, then **c*** of most of the chlorite and lizardite in Figure 5 occurs at an angle of about 50° with respect to **a*** of enstatite. However, a small portion of intercalated talc, brucite, and serpentine layers occurs in the topotactic orientation noted above. The orientation relationships in the augite lamellae are not preserved perfectly, as evidenced by the relative rotation of the two parts of the augite lamella in Figure 5. Such rotations are presumably the result of deformation.

In general, the augite exsolution lamellae have not been altered except for minor nanometer-scale regions on the

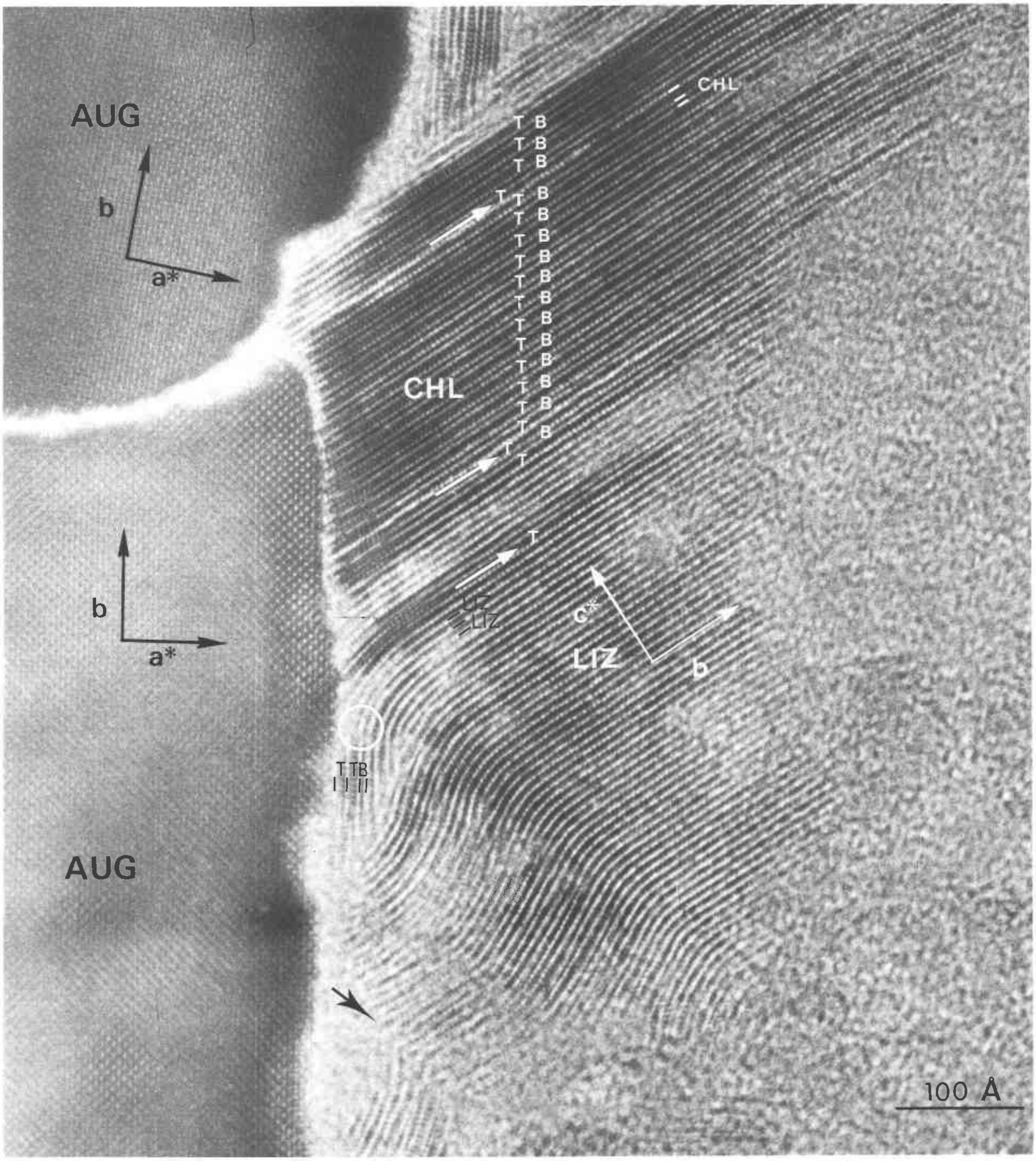

Fig. 5. HRTEM image of chlorite (CHL) and lizardite (LIZ) next to an augite exsolution lamella (AUG). Intercalated talc-like layers (T) are indicated by white arrows. Brucite-like layers are indicated by (B). Near the interface, the serpentine layers are curved, and the black arrow indicates a circumflex structure.

edges of the lamellae. In Figure 6, the preexisting enstatite has been completely pseudomorphosed, and augite has been partially replaced by a short segment of one brucite-like and three talc-like layers parallel to (001) of augite.

In intensely altered regions of the porphyroblast, incomplete polygonal serpentine structures have been found (Fig. 7). These structures are similar to those observed in bastite by Cressy and Zussman (1976), and those in veins and synthetic samples by Jiang and Liu (1984), Mellini (1986), and Yada and Liu (1987). The cores of these po-

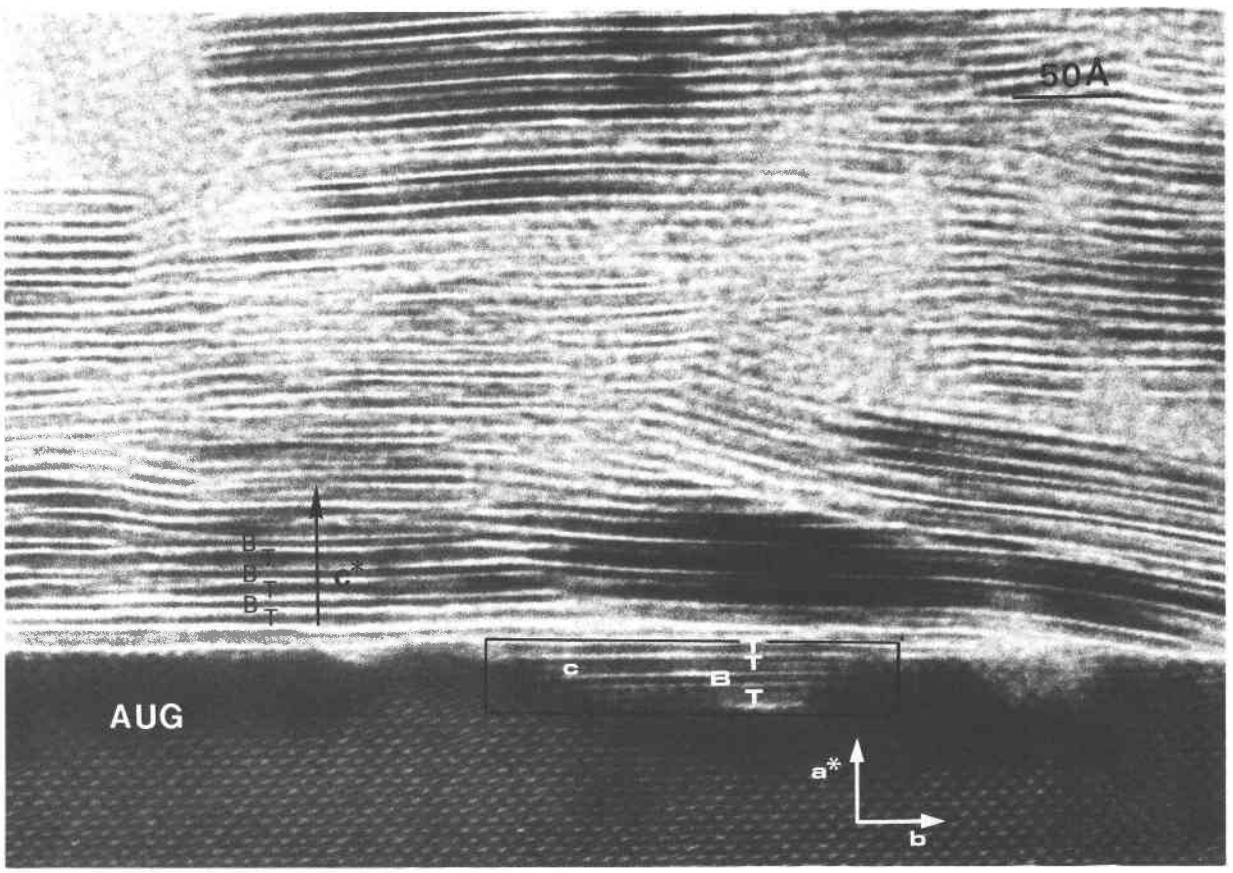

Fig. 6. HRTEM image of a slightly altered augite exsolution lamella. The enstatite host has been completely replaced (see text).

lygonal structures do not seem to consist of normal chrysotile fibers. Similar polygonal serpentine has been found in the altered matrix and is discussed below.

Matrix alteration

Microcrystalline enstatite in the matrix has been completely serpentinized. As shown in Table 1 (analysis 5), the average matrix serpentine composition is similar to that of the topotactic-lizardite pseudomorphs of the enstatite porphyroblasts. Low-magnification electron micrographs of serpentine (Fig. 8a) show that two forms of organization of the serpentine minerals are present: (1) nearly perfect equilateral triangles (labeled TRI) with each side 5 to 10 μm long; and (2) incomplete polygonal serpentine structures (labeled P) composed of 4 to 10 sectors (Figs. 7 and 8a). The inset SAED pattern (Fig. 8b) illustrates that the **c*** directions of two of the adjacent sectors of the incomplete polygonal structure in Figure 8a are tilted by about 14° in the plane of the image. AEM analyses indicate that polygonal serpentines (Table 4, analyses 25–28) contain similar Al but higher Fe contents than the topotactic lizardites. Thus, the growth of planar (versus polygonal) serpentine does not seem to depend on Al content in this sample.

The SAED pattern from the intersection of six of the triangular structures (Fig. 8c) shows six indistinct groups of equidistant reflections on the inside ring, suggesting three preferred orientations. In HRTEM images, these triangular structures appear to consist of randomly distributed packets of 10–25 anastomosing or overlapping lizardite layers. They commonly occur with tapered chlorite-layer packets. Al and Fe contents of the triangular lizardite are identical within analytical error to those in planar topotactic lizardite.

Electron microprobe analyses of serpentine containing high densities of grain boundaries exhibit abnormally high TiO_2 and CaO contents (Table 1, analysis 6). TEM images and AEM analyses have been used to identify titanite inclusions, 500–1800 Å in diameter, typically grouped in rosettes (Table 4, analysis 29), which explains this unusual composition.

Summary of orientation relationships

A schematic diagram summarizing the textural relations between enstatite and its alteration products is presented in Figure 9. In the interior zones of enstatite porphyroblasts, topotactic lizardite dominates with $(001)_{liz} \parallel (100)_{en}$. In porphyroblasts that are intensely altered, ran-

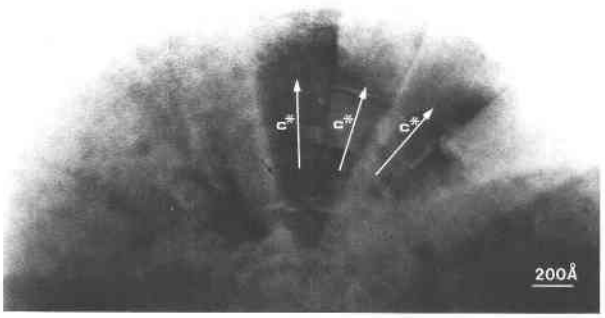

Fig. 7. Lattice image of an incomplete polygonal serpentine fiber composed of continuous lizardite layers with changes in orientation between the sectors.

domly oriented lizardite coexisting with polygonal serpentine and chlorite typically are found. These alteration products, along with interstratified extra talc- and brucite-like layers, chrysotile, and curved serpentine, also are commonly found in random orientations near augite lamellae (Fig. 10).

In the matrix, randomly oriented lizardite packets, polygonal serpentine, and chlorite-like layers dominate. There is no evidence that the pyroxene crystals in the fine-grained matrix have any control over lizardite orientation. Therefore, nontopotactic lizardite has been observed in three distinct alteration sites (matrix, highly altered porphyroblasts, and near augite lamellae), whereas topotactic lizardite is restricted to the interior portions of enstatite porphyroblasts.

TABLE 4. Structural formulae of enstatite, augite exsolution lamellae, and serpentine, calculated from AEM analyses

	Si	Mg	Fe^{2+}	Al	K	Ca	Ti	Cr	Mn	Ni	Na
1	1.84	1.60	0.31	0.23	—	0.01	—	—	0.01	—	—
2	1.86	1.60	0.29	0.21	—	0.01	0.01	0.02	0.01	—	—
3	1.77	1.67	0.28	0.25	0.01	0.01	—	0.03	0.01	0.01	0.11
4	1.80	1.75	0.25	0.21	0.01	—	—	0.01	0.01	—	0.08
5	1.91	1.77	0.22	0.11	—	0.01	—	—	0.01	—	—
6	1.81	1.74	0.21	0.28	—	0.01	—	—	0.01	—	—
7	1.80	1.75	0.21	0.25	0.01	—	—	0.01	0.01	0.01	—
8	1.89	1.72	0.20	0.19	—	—	—	—	—	—	—
9	1.93	0.76	0.08	0.27	—	0.81	0.01	0.02	—	0.01	—
10	1.97	0.70	0.10	0.28	—	0.77	0.01	0.01	—	—	0.09
11	1.72	2.35	0.43	0.50	—	—	—	0.01	0.01	0.01	—
12	1.80	2.21	0.36	0.51	—	—	—	0.01	0.01	0.02	—
13	1.83	2.10	0.37	0.52	0.04	0.01	—	0.02	0.01	0.03	—
14	1.80	2.49	0.22	0.45	—	0.01	—	—	—	0.01	—
15	1.67	2.37	0.23	0.69	—	0.01	—	—	—	—	—
16	1.82	2.43	0.30	0.40	—	—	—	0.01	0.01	0.01	—
17	1.76	2.62	0.26	0.39	—	—	—	—	—	0.01	—
18	1.77	2.50	0.27	0.45	0.01	—	—	—	—	0.01	—
19	1.76	2.38	0.23	0.55	0.01	0.01	—	0.01	—	0.01	—
20	1.82	2.50	0.37	0.33	—	—	—	—	—	—	—
21	1.84	2.47	0.35	0.33	—	—	—	—	—	—	—
22	1.71	2.52	0.34	0.48	—	—	—	—	—	—	—
23	1.81	2.58	0.30	0.32	—	—	—	—	—	—	—
24	1.79	2.57	0.34	0.32	—	0.01	—	0.01	0.01	—	—
25	1.80	2.33	0.27	0.54	—	—	—	—	—	—	—
26	1.77	2.27	0.26	0.60	0.01	—	0.02	0.01	—	—	—
27	1.69	2.24	0.59	0.53	—	—	—	0.01	—	—	—
28	1.76	2.17	0.67	0.42	—	—	—	0.01	—	—	—
29	1.09	0.09	—	0.04	0.90	—	—	—	—	1.09	—

Note: 1–8: Enstatite (formulae based on 6 O); 9–10: Augite exsolution lamellae (formulae based on 6 O); 11–19: Topotactic lizardite after enstatite porphyroblasts (formulae based on 7 O); 20–24: Serpentine after enstatite neoblasts (formulae based on 7 O); 25–28: Polygonal serpentine (formulae based on 7 O); 29: Titanite granules (formulae based on 5 O).

DISCUSSION

Relationships between enstatite and its alteration products and the degree of system openness

Yau et al. (1987) observed that during smectite-to-illite reactions, illite layers may have a crystallographically controlled orientation relationship with respect to the smectite precursor in shales with low porosity and permeability. However, Yau et al. found that illite in shales with high permeability and porosity tended to occur as individual euhedral to subhedral crystals. Referring to this study, Wicks (1986) suggested that the amount of water available for bastite formation may have an influence on the orientation of the alteration products.

Similar conclusions may be drawn from the Pernes data. The availability of water on a micrometer scale may affect the local orientation of serpentine minerals. The nontopotactic serpentines and other sheet silicates developed in the matrix, near fractures, and in areas of high dislocation density. In the matrix where grain boundaries, microcracks, and other forms of microporosity were abundant, water had easy access to alteration sites, and there was a large surface area available for reaction. The reaction presumably proceeded relatively rapidly, and the amount of fluid available for the reactions was not a limiting factor. In the same way, zones near fractures in the porphyroblasts became intensely altered because of high fluid flow. Incoherent interfaces and dislocations at semicoherent interfaces, such as those found at the boundaries of augite exsolution lamellae, acted as fluid-flow channels parallel to $[001]_{en}$ but should have experienced lower fluid fluxes than in the matrix and porphyroblast fractures. In contrast, the interiors of large, unfractured porphyroblasts represent regions of more restricted fluid flow. Here, topotactic lizardite dominates.

The restriction of the amount of fluid available for reaction carries several implications. Assuming that flow rates are slowed down in closed regions, restricted fluid flow would allow more time for equilibrium between rock and fluid to be achieved and therefore reduce the dissolution capabilities of the fluid by saturating the fluid with respect to the nearby minerals. Diffusion may become the dominant form of cation transport in these regions. Increased residence time of fluids would allow for reactions with slow rates to take place, such as the growth of larger crystals, crystals with fewer defects, precipitation of phases from fluids with low degrees of supersaturation. A restricted fluid flow and increased fluid residence time may be necessary for the higher degree of organization required of topotactic reactions, in which the interface between the reactant and product structures is extremely tight and the reaction is likely to be diffusion-limited. The

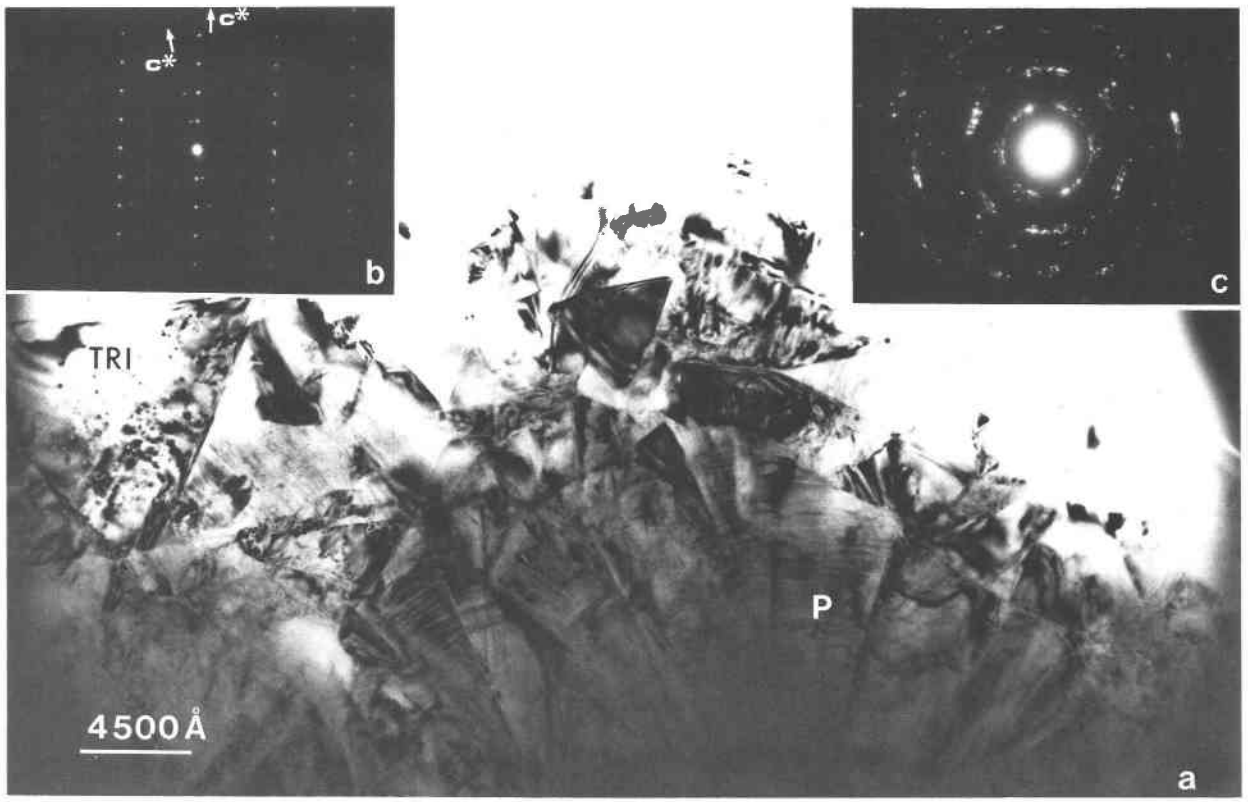

Fig. 8. Serpentine texture in the microcrystalline matrix. (**a**) Low-magnification TEM image of triangular structures (TRI) intergrown with polygonal serpentine fibers (P). (**b**) SAED pattern from two adjacent sectors of a polygonal serpentine fiber, showing the orientation change of the (001) planes across their boundary. (**c**) SAED pattern from six adjoining triangular domains.

lessened availability of reactants may also necessitate the incorporation of parts of the host structure. Thus, we suggest that the diffusion of cations into and away from the restricted pyroxene-serpentine interface is the limiting step for topotactic lizardite, rather than nucleation or growth rates.

In more open systems, the abundant fluid becomes the dominant medium for cation transport and lower fluid-residence times allow for greater dissolution capabilities. The fine-grained nature of the matrix lizardite suggests that nucleation rates were greater than growth rates. Thus, the randomly oriented lizardites crystallized from solution by a neoformation reaction and needed no template for precipitation to occur.

Other TEM studies report observations that corroborate a relationship between orientation and fluid flux. Cressey and Whittaker (1982) describe anthophyllite altering to chlorite and serpentine. Along very narrow cracks, (001) of the sheet silicates is roughly parallel to (210) of the amphibole, whereas chlorite develops without any orientation relationship in wider cracks. Eggleton and Boland (1982), in a study of enstatite weathering to talc and Fe oxides, describe the first stage of weathering as a topotactic, solid-state transformation of orthopyroxene into biopyroboles and talc-like layer silicates. With increasing weathering and, most likely, a larger fluid flux, layer silicates with less rigorous topotactic relationships replace the initial talc-like phase and appear to fill in holes and cracks in the orthopyroxene without any crystallographic relationship.

Different alteration products can aid in producing more restricted microenvironments. Eggleton (1986) emphasized the importance of the degree of similarity of host and alteration product structures on weathering rates. Those products having structures that fit well with the host will have fewer defects in their boundaries during topotactic reactions. This would further restrict the fluid flow along that boundary. In the current study, topotactic talc-like layers produce fewer defects than do topotactic lizardites. Therefore, talc reduces alteration rates.

The mineral assemblage of the Pernes alteration products may also be dependent upon fluid flux at the local reaction site. In relatively closed microsites, enstatite is replaced predominantly by lizardite. When the openness of the reaction microsite to fluids increases, a wide variety of products, including lizardite layers, chrysotile, curved and polygonal serpentine, talc-like and brucite-like layers, and chlorite, crystallize. Since all of these materials are essentially in the MgO-FeO-SiO_2-H_2O system, this suggests that the more open sites promote the crys-

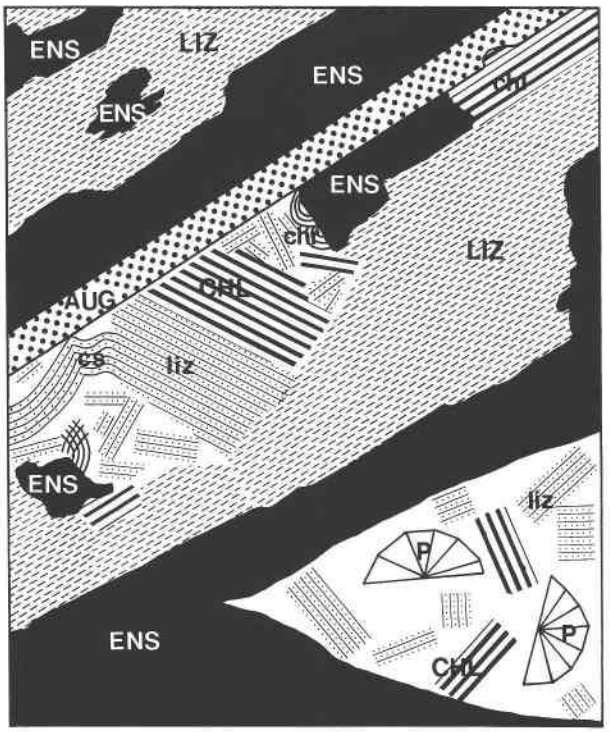

Fig. 9. Diagram summarizing the mineral assemblage and orientations and positions of the alteration products in the enstatite porphyroblasts. ENS = enstatite; AUG = augite; LIZ = topotactic lizardite; liz = nontopotactic lizardite; chr = chrysotile; cs = curved serpentine structures; CHL = chlorite; chl = chlorite-like layer; P = polygonal serpentine.

tallization of a very diverse, thermodynamically metastable assemblage.

Enstatite-topotactic lizardite reaction chemistry

Lattice-fringe images such as that in Figure 4 show that five (001) topotactic-lizardite fringes generally replace two orthopyroxene (100) fringes. As the magnitudes of the enstatite unit-cell parameters *b* and *c* are nearly equal to the lizardite *b* and *a* parameters, respectively (Table 3), two enstatite cells may be replaced by five lizardite cells with a 4.7% volume increase. This nearly isovolumetric reaction can be balanced based on averages of AEM analyses in Table 4 (analyses 1–8 and 11–19), neglecting elements that are considered below the detection limit. The cation budget for this reaction can be approximated by the reaction $32(Mg_{0.85}Fe^{2+}_{0.12}Al_{0.03})(Si_{0.92}Al_{0.08})O_3 + 41.46H_2O + 4.04H + 1.48Al \rightarrow 10(Mg_{2.38}Fe^{2+}_{0.30}Al_{0.27})(Si_{1.77}Al_{0.23}O_5)(OH)_4 + 11.74H_4SiO_4 + 3.40Mg + 0.84Fe + 0.25O_2$. The valence and speciation conventions of Carmichael (1969), as applied by Veblen and Ferry (1983), have been used to write this reaction.

The above reaction implies a loss of approximately 40% Si, 10% Mg, and 20% Fe, and a net gain of 40% Al. The Fe liberated to the fluid can be incorporated in the chlorite structures and in Fe-Ni sulfides that have been observed with the SEM. No Fe oxides have been found. The reaction also requires addition of Al from a source other than the pyroxenes. Large areas of chlorite also require more Al than can be supplied by the pyroxenes.

The alteration of ferroan spinel and chromite releases Al, but this Al is immediately integrated into surrounding lizardite (Le Gleuher, 1987). This lizardite, containing about 26% Al_2O_3 by weight, is confined to a border around the spinel 40 to 200 μm wide, indicating that Al migrates from this reaction only a short distance. Therefore, spinel alteration cannot supply the necessary Al required by topotactic lizardite formed further away than a few hundred micrometers. This is somewhat problematical, given the relative immobility of Al in normal hydrothermal fluids. This may suggest that the nearly constant-volume reaction mechanism suggested by the textures of intergrown enstatite and topotactitic lizardite is not obeyed throughout the entire topotactic reaction process.

If the reaction that forms the randomly oriented lizardite conserves Al, calculations indicate that there would be a 25% reduction in volume. Yet, optical and electron microscope observations suggest that the pseudomorphic reaction producing the Pernes bastite does not produce significant porosity and therefore should be nearly isovolumetric. The most likely sources for the additional Al are the fluids that created the many plagioclase and potassium feldspar veins that cut the massif des Pernes; one such vein is very close to the studied outcrop. However, it is not possible to determine rigorously the various sources and sinks for Al from our observations.

Conclusions

From observations of altered pyroxenes from the massif des Pernes, we conclude that the availability of altering fluids may have a profound effect on the type of reaction mechanism that produces pseudomorphing serpentine. Reactions producing topotactic lizardite are a result of restricted fluid flow in diffusion-controlled regions. Random fine-grained serpentines and other reaction products are a result of a dissolution-neoformation mechanism that occurs where the system is more open and fluid flux is high. Both mechanisms can occur side by side over a very small scale. We thus concur with previous authors (e.g., Yau et al., 1987; Wicks, 1986) who suggest that variations in alteration reaction mechanisms that produce sheet silicates can result from different environments having different access to the altering fluid.

Acknowledgments

The authors would like to thank Gerard Spinnler and an anonymous reviewer for helpful comments. Support from the Laboratoire de Pétrologie de la Surface at the Faculté des Sciences, Poitiers, from the Université de St-Jérôme, Marseille, and from ORSTOM, France, is gratefully acknowledged. High-resolution and analytical electron microscopy were supported by NSF grants EAR86-09277 and EAR89-03630, and the electron microscopy facilities at Johns Hopkins were established with partial support from EAR83-00365.

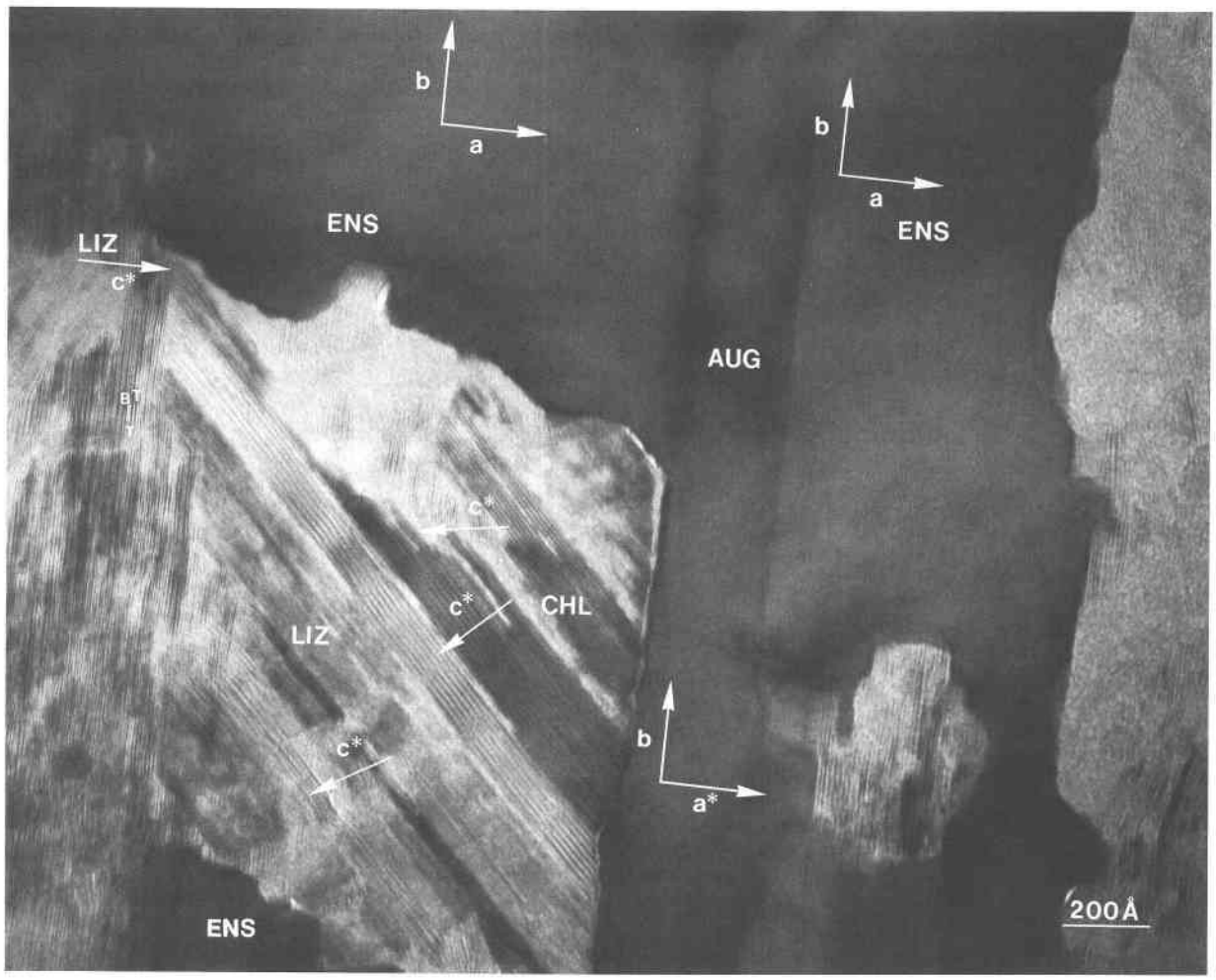

Fig. 10. HRTEM image showing intergrowths of nontopotactic lizardite (LIZ) and chlorite (CHL) near an augite (AUG) exsolution lamella. Further from the lamella, lizardite, talc-like (T), and brucite-like (B) layers are in topotactic orientation, with (001) parallel to (100) of the enstatite (ENS).

REFERENCES CITED

Buseck, P.R., Nord, G.L. Jr., and Veblen, D.R. (1980) Subsolidus phenomena in pyroxenes. Mineralogical Society of America Reviews in Mineralogy, 7, 117–211.

Carmichael, D.M. (1969) On the mechanism of prograde metamorphic reactions in quartz-bearing pelitic rocks. Contributions to Mineralogy and Petrology, 20, 244–267.

Chernosky, J.V. Jr. (1975) Aggregate refractive indices and unit cell parameters of synthetic serpentine in the system MgO-Al_2O_3-SiO_2-H_2O. American Mineralogist, 60, 200–208.

Colin, F., Noack, Y., Trescases, J.J., and Nahon, D. (1985) L'altération latéritique débutante des pyroxénites de Jacuba, Niquelandia, Brésil. Clay Minerals, 20, 93–113.

Cressey, B.A. (1977) Electron microscopic studies of serpentinites. Ph.D. thesis, Manchester University, England.

——— (1979) Electron microscopy of serpentine textures. Canadian Mineralogist, 17, 741–756.

Cressey, B.A., and Whittaker, E.J.W. (1982) Morphology and alteration of asbestiform grunerite and anthophyllite. Mineralogical Magazine, 46, 77–87.

Cressey, B.A., and Zussman, J. (1976) Electron microscopic studies of serpentines. Canadian Mineralogist, 14, 307–313.

Deer, W.A., Howie, R.A., and Zussman, J. (1978) Rock-forming minerals, vol. 2A, Single-chain silicates, 668 p. Wiley, New York.

Delvigne, J. (1983) Micromorphology of the alteration and weathering of pyroxenes in the Koua Bocca Ultramafic intrusion, Ivory Coast, Western Africa. In D. Nahon and Y. Noack, Eds., Petrology des alterations et des sols, Mémoires sciences geologiques, Strasbourg, 72, 57–68.

Dungan, M.A. (1979) A microprobe study of antigorite and some serpentine pseudomorphs. Canadian Mineralogist, 17, 771–784.

Eggleton, R.A. (1986) The relation between crystal structure and silicate weathering rates. In S. Colman and D. Dethier, Eds., Rates of chemical weathering of rocks and minerals, p. 21–40. Academic Press, Orlando, Florida.

Eggleton, R.A., and Boland, J.N. (1982) Weathering of enstatite to talc through a sequence of transitional phases. Clays and Clay Minerals, 30, 11–20.

Frost, B.R. (1975) Contact metamorphism of serpentinite, chloritic blackwall and rodingite at Paddy-Go-Easy Pass, Central Cascades, Washington. Journal of Petrology, 16, 272–313.

Ikin, N.P., and Harmon, R.S. (1983) Mineralogy and petrology of the

Highland Border Suite Serpentines. Mineralogical Magazine, 47, 301–310.

Jahanbagloo, I.C., and Zoltai, T. (1968) The crystal structure of a hexagonal Al-serpentine. American Mineralogist, 53, 14–24.

Jiang, S., and Liu, W. (1984) Discovery and its significance of Povlen type hydrochrysotile. Acta Geologica Sinica, 58, 136–142 (in Chinese, abstract in English).

Le Gleuher, M. (1987) Alteration hydrothermale des pyroxenes (serpentines, talc, amphiboles); influence du degré d'ouverture du système d'altération; apports de la microscopie électronique par transmission à haute-resolution. Thèse Doctorat en Sciences, Université d'Aix-Marseille III, France, 127 p.

Livi, K.J.T., and Veblen, D.R. (1987) "Eastonite" from Easton, Pennsylvania: A mixture of phlogopite and a new form of serpentine. American Mineralogist, 72, 113–125.

Mellini, M. (1982) The crystal structure of lizardite 1*T*: Hydrogen bonds and polytypism. American Mineralogist, 67, 587–598.

——— (1986) Chrysotile and polygonal serpentine from the Balangero serpentinite. Mineralogical Magazine, 50, 301–305.

Nahon, D., and Colin, F. (1982) Chemical weathering of orthopyroxenes under lateritic conditions. American Journal of Science, 282, 1232–1243.

Nakajima, Y., and Ribbe, P.H. (1980) Alteration of pyroxenes from Hokkaido, Japan, to amphibole, clays, and other biopyriboles. Neues Jahrbuch für Mineralogie Monatshefte, 6, 258–268.

Oswald, H.R., and Günter, J.R. (1985) Structural relationships in heterogeneous solid state reactions. In P. Barret and L.-C. Dufour, Eds., Reactivity of solids, p. 101–108. Elsevier, Amsterdam.

Spinnler, G.E. (1985) HRTEM study of antigorite, pyroxene-serpentine reactions, and chlorite. Ph.D. thesis, Arizona State University, Tempe, Arizona, 248 p.

Tournarie, M. (1969) Programme d'affinement statistique, version K par régression non linéaire. Journal de Physique, 10, 737.

Veblen, D.R. (1980) Anthophyllite asbestos: Microstructures, intergrown sheet silicates, and mechanisms of fiber formation. American Mineralogist, 65, 1075–1086.

Veblen, D.R., and Buseck, P.R. (1979) Serpentine minerals: Intergrowths and new combination structures. Science, 206, 1398–1400.

——— (1980) Microstructures and reaction mechanisms in biopyriboles. American Mineralogist, 65, 599–623.

——— (1981) Hydrous pyriboles and sheet silicates in pyroxenes and uralites: Intergrowth microstructures and reaction mechanisms. American Mineralogist, 66, 1107–1134.

Veblen, D.R., and Ferry, J.M. (1983) A TEM study of the biotite-chlorite reaction and comparison with petrologic observations. American Mineralogist, 68, 1160–1168.

Velbel, M.A. (1987) Rate-controlling factors in the weathering of some ferromagnesian silicate minerals. Transactions, 13th Congress of the International Society of Soil Science, Hamburg, FRG, VI, 1107–1118.

Wicks, F.J. (1986) Lizardite and its parent enstatite: A study by X-ray diffraction and transmission electron microscopy. Canadian Mineralogist, 24, 775–788.

Wicks, F.J., and Plant, A.G. (1979) Electron-microprobe and X-ray-microbeam studies of serpentine textures. Canadian Mineralogist, 17, 785–830.

Wicks, F.J., and Whittaker, E.J.W. (1977) Serpentine textures and serpentinization. Canadian Mineralogist, 15, 459–488.

Yada, K., and Liu, W. (1987) Polygonal micro-structures of Povlen chrysotile observed by high resolution electron microscopy. Proceedings of the sixth meeting of the European Clay Group, Seville, Spain, 596–597.

Yau, Y.C., Peacor, D.R., and MacDowell, S.D. (1987) Smectite-to-illite reactions in Salton Sea shales: A transmission and analytical electron microscopy study. Journal of Sedimentary Petrology, 57, 335–342.

MANUSCRIPT RECEIVED JULY 1, 1989
MANUSCRIPT ACCEPTED APRIL 17, 1990